Engineering Nanostructures by Binding Single Molecules to Single-Walled Carbon Nanotubes

J. Joseph Sharkey, Samuel D. Stranks, Jian Huang, Jack A. Alexander-Webber, and Robin J. Nicholas*

Department of Physics, Clarendon Laboratory, Parks Road, Oxford OX1 3PU, United Kingdom

ABSTRACT Organic and hybrid organic—inorganic systems are promising candidates for low cost photovoltaics. Recently, perovskite-based systems have been attracting a large amount of research attention, where the highest performing devices employ a small molecule (2,2′,7,7′-tetrakis(*N*,*N*-di-*p*-methoxyphenyl-amine)-9,9′-spirobifluorene) (Spiro-OMeTAD) hole transporter. Here, we demonstrate the production of single-walled carbon nanotube (SWNT)/single molecule nanostructures using a simple solution processing technique for effective and strong binding of Spiro-OMeTAD to individual polymer-wrapped SWNTs. These small molecules bind very strongly, which causes both large mechanical strain of the nanotubes and also improves the separation of individual SWNTs, thus improving the nanotube photoluminescence quantum efficiency by 1 order of magnitude compared to simple polymer—nanotube nanohybrids. Using absorption and photoluminescence measurements, we show that there is a dramatic variation in the electronic properties of the polymer—NT nanocomposites due to the band alignment formed with Spiro-OMeTAD. These self-assembled nanocomposites offer the potential for integration into high performance optoelectronic such as photovoltaic cells and light emission devices.

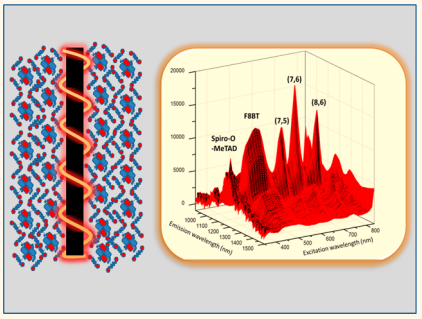

KEYWORDS: carbon nanotube · Spiro-OMeTAD · conjugated polymer · polymer wrapping · organic photovoltaics

Single-Walled Carbon Nanotubes (SWNTs) are of great interest for use in Organic (OPV) and hybrid photovoltaic solar cells due to their combination of attractive properties such as high charge carrier mobilities,[1] long-lived charge transport characteristics,[2] large aspect ratios, and high tensile strength.[3] Several research groups have recently reported that SWNTs, depending on the dopants, can act as efficient electron accepting materials,[4−6] good absorbers,[7] and excellent hole transporting materials,[8,9] demonstrating their promise for use in photovoltaics. Nanotubes have also recently been integrated as hole transporters into high performance perovskite-based solar cells, both as bundled tubes with mixtures of single- and multiwalled tubes,[10] and very successfully as individual polymer-wrapped tubes.[11,12]

By wrapping SWNTs with a wide range of π-conjugated polymers, we can efficiently modify both the electronic and mechanical properties of the nanotubes while also dispersing the tubes to avoid unwanted bundling. The binding is mainly due to the strong $\pi-\pi$ interactions which lead to highly efficient nanotube dispersions.[13] The noncovalent nature of the polymer binding to the nanotube is of great advantage because we not only make use of the favorable properties of the polymers but also retain the properties of the nanotubes. Recently, Schuettfort *et al.*[14] showed that smaller diameter nanotubes coated with a small bandgap polymer can also form Type-II heterojunctions. In another recent work, Stranks *et al.*[15,16] showed that the binding of two polymers (F8BT and P3HT) can be manipulated in order to produce new nanotube-dual polymer heterostructures which have potential applications in solar cells. Alternatively, Porphyrins can also be used to bind to the nanotubes *via* $\pi-\pi$ stacking.[17] The Porphyrin binding is sufficiently strong to not only cause strain to the nanotubes but also significantly affect their electronic properties.[18]

In this report, we investigate the binding of nanotubes to Spiro-OMeTAD, which is an amorphous conjugated small, organic material initially used as a hole transporting material in solid state dye-sensitized solar cells[19] but more recently in perovskite-based

* Address correspondence to r.nicholas1@physics.ox.ac.uk.

Received for review October 14, 2014 and accepted December 1, 2014.

Published online December 01, 2014
10.1021/nn505860a

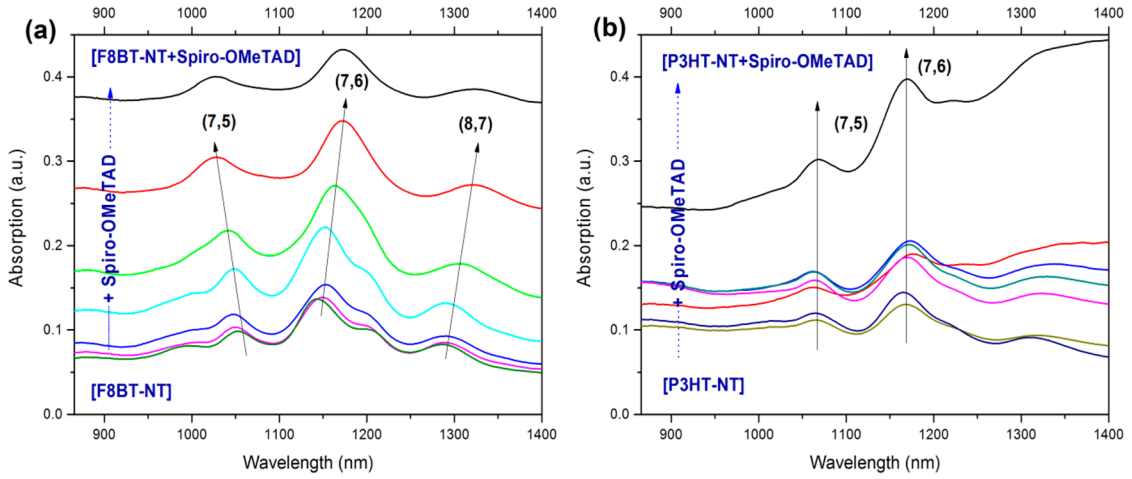

Figure 1. Absorption spectra of nanohybrid films with increasing concentration of Spiro-O-MeTAD added to precursor solutions of (a) [F8BT-NT] and (b) [P3HT-NT].

solar cells, which have achieved power conversion efficiencies exceeding 19%.[20−24] We fabricate a novel complex nanostructure prepared by first wrapping SWNTs with a monolayer of semiconducting polymer (F8BT/P3HT) that forms Type-I/Type-II heterojunctions with the nanotube, and subsequently binding a large number of small molecules (Spiro-OMeTAD) onto the [polymer−NT] nanohybrids. We use absorption and photoluminescence excitation (PLE) measurements to show that the small molecules induce a mechanical strain on the nanotubes. Further, atomic force (AFM) and scanning electron (SEM) microscopy show that Spiro-OMeTAD binds strongly to Polymer-NT nanohybrids, forming very thick coatings and leading to additional debundling of the tubes.

RESULTS AND DISCUSSION

First, we functionalized the SWNTs with either F8BT or P3HT by tip-sonicating appropriate amounts of CoMoCAT SG76 SWNTs and polymer materials using methods described elsewhere.[15,25,26] The unwrapped nanotubes and other unwanted material were removed as a residue upon centrifugation of the mixture, while the polymer-dispersed tubes (nanohybrids) were retained in the supernatant. These nanohybrids were subjected to a simple solution processing technique in order to remove the excess unused polymers in solution.[25] Various concentrations of Spiro-OMeTAD were then added to these 100% pure (excess polymer removed) polymer-NT solutions and the material was drop-cast on to plasma-etched quartz substrates (see Methods for full details).

Absorption measurements for [F8BT-NT] films in the NIR region are shown in Figure 1a. They reveal three distinctive peaks that are attributed to the first van Hove bandgap E_{11} at 1053, 1145, and 1281 nm corresponding to (7, 5), (7, 6), and (8, 7) chirality tubes with diameters 0.82, 0.89, and 1.03 nm, respectively.[27] These peaks are red-shifted relative to the [SDBS-NT] samples due to the dielectric screening effect on the SWNT caused by the F8BT.[14] When an increasing concentration of Spiro-OMeTAD is added to the F8BT-coated nanotubes the absorption peaks are either red- or blue-shifted, depending on the nanotube family.[19] By contrast, Figure 1b shows that no significant shifts are observed when Spiro-OMeTAD is added to [P3HT-NT] nanohybrids.

The family dependent shifts suggest strain-induced changes in the band structure of individual single-walled carbon nanotubes, as has been observed earlier for nanotubes which have been strained by freezing,[28] or wrapping with polymers or large molecules.[18,29] The energy shifts of the E_{11} bands depend on both the chiral indices and the magnitude of the strain in the radial and azimuthal directions[30] so that it is possible to deduce the separate strain components by measuring nanotubes with different chiral indices.

Increased spectral resolution for tubes with different chiral indices can be obtained by resonant excitation into the E_{22} states using photoluminescence excitation (PLE) spectroscopy, which is a powerful tool to investigate the degree of bundling in nanotubes, assign nanotube species, and determine any associated peak shifts.[31] Figure 2a,b shows PLE false color contour maps for the [F8BT-NT] and [F8BT-NT]-Spiro-OMeTAD samples, respectively. The excitation range of 600−800 nm shows E_{11} emission peaks resulting from direct excitation into the E_{22} transitions of six different semiconducting species [(7, 5), (7, 6), (8, 4), (8, 6), (8, 7) and (9, 4)] of SWNTs, while excitation around 480 nm shows E_{11} emission resulting from energy transfer from the polymer to the nanotube following absorption in F8BT.[15,32] In the [F8BT-NT]-Spiro-OMeTAD films, the emission peaks of three semiconducting nanotube species belonging to the family, q = +1, namely (7, 6), (8, 4) and (8, 7), are progressively red-shifted with the increasing concentration of Spiro-OMeTAD (see Supporting Information), whereas the emission peaks of three other

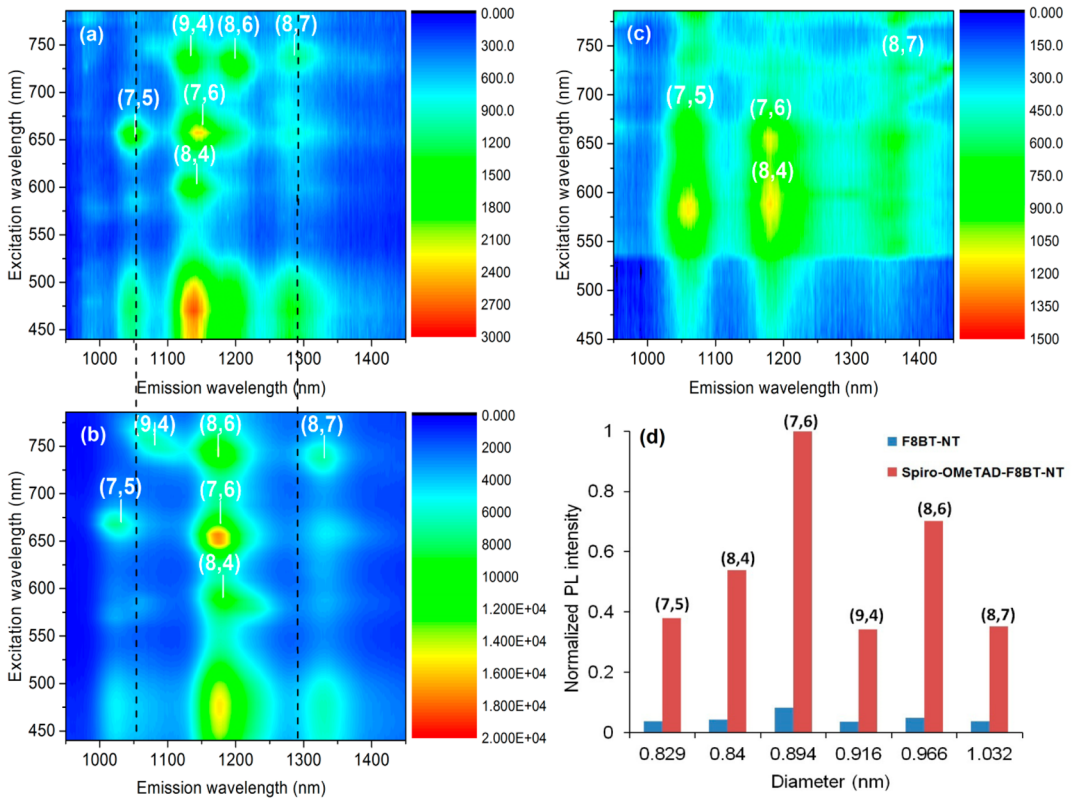

Figure 2. PLE maps of the purified nanohybrid films (on a quartz substrate) composed of (a) [F8BT-NT], (b) [F8BT-NT] + 50 mg Spiro-O-MeTAD, and (c) [P3HT-NT] + 50 mg Spiro-O-MeTAD. The resonant nanotube species transitions are labeled in white. Nanotube species were assigned from Weisman and Bachilo,[27] red-shifted by 25 meV for F8BT and 50 meV for P3HT.[14] (d) Comparison of PL intensities of various SWNT species by exciting them at their respective wavelengths in both [F8BT-NT] and [F8BT-NT] + 50 mg Spiro-O-MeTAD samples.

semiconducting species that belong to the family $q = -1$, namely (7,5) (8,6), and (9,4) nanotubes, are blue-shifted. This phenomenon is attributed to the very strong binding of Spiro-OMeTAD to the nanohybrids causing a very large mechanical strain in the SWNTs.[18]

In addition, the intensity of the nanotube photoluminescence from the Spiro-O-MeTAD-[F8BT-NT] nanohybrid increases by ~1 order of magnitude compared to the unwrapped [F8BT-NT] in films (Figure 2d). We suggest that this is caused by improved debundling of the agglomerated tubes due to the very strong binding by Spiro-O-MeTAD, which leads to the formation of large, well separated nanohybrids as seen in the microscopy reported below. The thick wrapping layer which we will show is formed by the Spiro-OMeTAD will also act to isolate the nanotubes from each other and from disorder present on the substrate. It is also possible that the electronic properties of the Spiro-O-MeTAD will play a role as the energy levels shown in Figure 5 suggest that it will provide additional electron confinement to reduce any charge loss when excitation is directly into the nanotubes. Direct excitation into the F8BT may be less effective however due to hole transfer into the Spiro-O-MeTAD, and it is noticeable that the F8BT energy transfer peaks around 480 nm become less strong relative to the direct E_{22} excitation.

By contrast, in the case of the P3HT-NT and P3HT-NT-Spiro-OMeTAD samples no significant peak shifts are observed and there is no change in the PL intensity (Supporting Information Figure S1 and Figure 2 c), leading us to the conclusion that the nanohybrids are still bundled and there is less physical interaction between Spiro-OMeTAD and [P3HT-NT] compared to [F8BT-NT] nanohybids.

Strain-induced changes in the band gaps of carbon nanotubes are well understood, giving a change in band gap (ΔE_{strain}) due to mechanical strain of[18,33−35]

$$\Delta E_{strain} = \left(\frac{2t_0 a_{c-c}}{d}\right)(\varepsilon_\perp - \nu\varepsilon_{||}) + 3qt_0[((1+\nu)\varepsilon_{||}\cos 3\theta + \varepsilon_\perp \sin 3\theta)] \quad (1)$$

where t_0 is the carbon−carbon transfer integral, a_{c-c} is its corresponding bond length, d is the diameter of the carbon nanotube. ν is the Poisson ratio, θ is the tube chiral angle, q is the nanotube species (±1) and $\varepsilon_{||}$ and $\varepsilon_\perp$ are the uniaxial and torsional strain components caused by the binding of the Spiro-OMeTAD to the [F8BT-NT] nanohybrids. The parameters used in our calculations are t_0 = 3.0 eV, a_{c-c} = 1.432 Å, ν = 0.2 and the average diameter of the nanotube is taken as d = 0.9 nm.[18] Fits to eq 1 are shown in Figure 3a and for the highest concentration of Spiro-OMeTAD yield

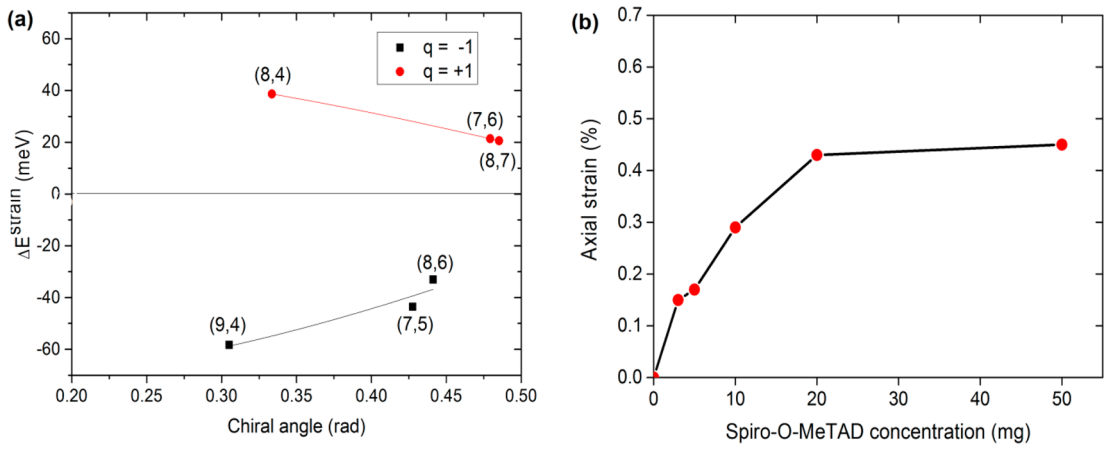

Figure 3. (a) Strain components for [F8BT-NT] + 50 mg Spiro-O-MeTAD composites. Curves show fits to the data using the Yang and Han[18,30] model for small strain with the constant term in eq 1. (b) Variation of axial strain values of the nanotubes in [F8BT-NT-Spiro-OMeTAD] nanostructures as a function of the concentration of Spiro-O-MeTAD.

values for $\varepsilon_{||}$(uniaxial strain) and $\varepsilon_{\perp}$(torsional strain) of 0.45% and 0.25%, respectively, which are significantly larger than the values observed previously from temperature- or pressure-induced strain effects[28] or from the binding of porphyrin units ($\varepsilon_{||} \sim 0.2\%$ and $\varepsilon_{\perp} \sim 0.1\%$).[18] The magnitude of the strain is found to increase significantly with the increasing Spiro-OMeTAD concentration, as shown in Figure 3b, which we attribute to a progressive increase in the thickness of the coating layer until this saturates at concentrations above 20 mg.

To investigate the morphology of the nanohybrids, thin films of [SWNT-Polymer] and [SWNT-Polymer]-Spiro-OMeTAD nano, hybrid structures were also drop-cast onto silicon substrates from diluted nanohybrid solutions. The height profiles of [F8BT-NT] and [P3HT-NT] films, along the cross section, show a typical height of 2−3 nm, corresponding to the height of a SWNT bound by either a monolayer or bilayer of polymer, separated by twice the van der Waals radius of carbon.[15,25] A three-dimensional AFM image of [F8BT-NT]-Spiro-OMeTAD film is shown in Figure 4a, revealing a uniform and thick coating of Spiro-OMeTAD over the entire length of the nanotubes, which prevents the formation of nanotube bundles. These nanohybrids are widely dispersed over the entire surface of the film. The height analysis shows that the diameter of these nanohybrids varies from 8 to 10 nm, indicating the formation of very thick coatings along the entire length of the nanotube. Typical nanotube lengths are between 0.5 and 2 μm long with a few longer tubes (8 μm), as shown in Figure 4a. Figure 4b shows an AFM image from the [P3HT-NT]-Spiro-OMeTAD films. This shows that the nanohybrids are more bundled with a typical height of 5−6 nm. In addition, we observe the formation of large crystals with a typical height of 10−15 nm which are speculated to be due to the nucleation of Spiro-OMeTAD by the P3HT.

SEM images for the same samples were also taken. Figure 4c shows the SEM of a [F8BT-NT]-Spiro-OMeTAD film. The black spherical structures are speculated to be Spiro-OMeTAD and the widely dispersed individual tubular structures on the silicon surface correspond to the [F8BT-NT]-Spiro-OMeTAD nanohybrids. The size of the [F8BT-NT]-Spiro-OMeTAD nanohybrids in this view is even larger with some structures up to 100 nm across in plan view. These widely dispersed nanohybrids are speculated to be the reason for the large improvement in PL intensity. The SEM image of [P3HT-NT]-Spiro-OMeTAD is shown in Figure 4d. As seen in the AFM analysis, the bundled P3HT-wrapped nanotubes are clearly visible, along with the large nucleated crystals of Spiro-OMeTAD. From the AFM and SEM analysis, the number of individual nanotubes and nanotube bundles is in a ratio of ∼1:10 for both the P3HT-NT and the P3HT-NT-Spiro-OMeTAD films. By contrast the ratio in the F8BT-NT films of ∼1:5 is transformed for the F8BT-NT-Spiro-O-MeTAD to 5:1, consistent with the order of magnitude increase in the PL emission intensity.

Our molecular dynamic simulations performed in our earlier work[14] with F8BT-NT nanohybrids show that the F8BT monomer units are generally quite rigid and the polymer does not wrap around the entire surface of the nanotube, leaving some "bare" regions without polymer. When Spiro-O-MeTAD is added to the [F8BT-NT] nanohybrids, we observe a decreased energy transfer from F8BT to NT, as noted in Figure 2b. This could suggest that Spiro-O-MeTAD displaces some of the F8BT surrounding the nanotube causing more "bare" NT patches, which leads to a direct binding of Spiro-O-MeTAD to some regions of the nanotube surface. We speculate that this initial layer of Spiro-O-MeTAD forms a seed onto which the additional Spiro-O-MeTAD molecules bind together, which results in large mechanical strain in the nanotube. In the case of [P3HT-NT] nanohybrids, we do not observe any

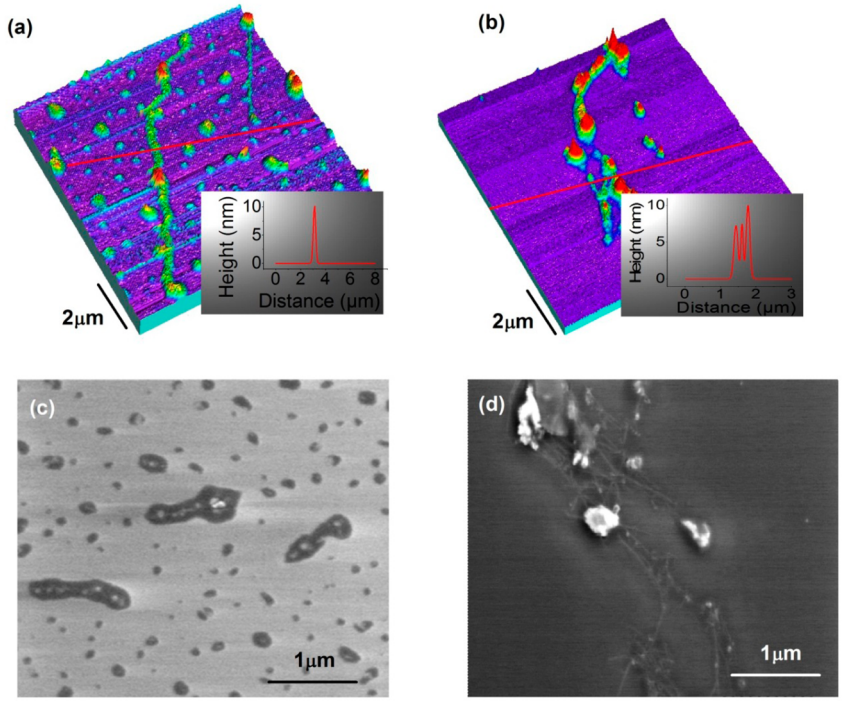

Figure 4. False color 3D AFM images of (a) [F8BT-NT] + 50 mg Spiro-O-MeTAD (b) [P3HT-NT] + 50 mg Spiro-O-MeTAD nanohybrid films casted by diluting the original solution to 1/1000 of the initial concentration, with corresponding SEM images shown in (c) and (d), respectively.

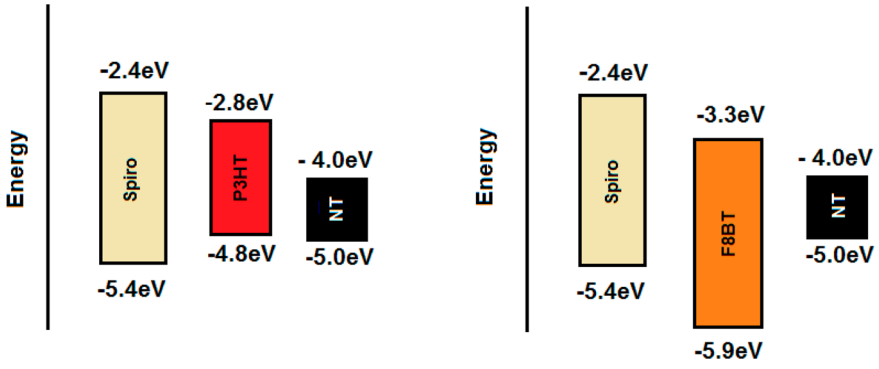

Figure 5. Schematic energy level diagram of nanohybrids consisting of P3HT/F8BT wrapped around the nanotube with Spiro-O-MeTAD embedded on them (Energies are given with respect to vacuum).[4,14]

variation in the energy transfer from P3HT to NT after the addition of Spiro-O-MeTAD (Figure 2c). We also know that P3HT binds more strongly to the nanotubes than F8BT and the P3HT chains are much more flexible and are able to cover the entire exposed nanotube surface.[14] Hence, we conclude that Spiro-O-MeTAD does not penetrate or remove the P3HT surrounding the nanotube and there is minimal direct physical interaction between Spiro-O-MeTAD and the NT.

Recently, Zhen Li *et al.*[10] reported the use of bundled SWNT/Spiro-OMeTAD composites as effective hole transporting materials for perovskite solar cells. Incorporation of these highly bundled composites improved the charge separation and collection in the solar cell and thereby doubled the power conversion efficiency from 5.14% to 9.90%. We have recently shown that a hole transporting layer consisting of either a SWNT:Spiro-OMeTAD composite[12] or a SWNT:insulating polymer composite[11] (where in both cases the tubes are partially debundled) can deliver power conversion efficiencies of over 15% in perovskite solar cells, along with greatly enhanced stability to moisture and thermal effects.[11] In the [F8BT-NT-Spiro] nanostructures, the interaction between F8BT and NT is reduced compared to the neat [F8BT-NT] structures, as some of the F8BT polymers are displaced by Spiro-O-MeTAD. This leads to direct interaction between Spiro-O-MeTAD and the nanotube. It is likely that the more controlled, designed and debundled structures presented here will allow further improvements over these existing reports. Our novel polymer/SWNT/Spiro-OMeTAD nanohybrids have complementary band alignments (Figure 5), which may

be useful in optimizing charge transport or separation in OPV devices or in confining photoexcitations (charges or excitons) for improved light emission devices. The work also opens up the possibility to exploit a wide range of other similar small molecules that could bind to the polymer-SWNT hybrids to allow designed engineering of new nanohybrids.

CONCLUSIONS

In conclusion, a novel complex nanostructure consisting of NT coated with the initial layer F8BT (with some regions of Spiro-OMeTAD), surrounded by excess Spiro-O-MeTAD, has been engineered and analyzed in detail. Absorption and PLE measurements show that the strong binding to the Spiro-OMeTAD results in large strains along both the uniaxial axis (0.45%) and the circumference (0.25%) of the nanotubes. AFM and SEM data show that Spiro-OMeTAD binds strongly to the entire surface of the nanotube forming very thick coatings and the nanohybrids can be widely dispersed onto film surfaces. This strong interaction leads to a significant improvement in PL emission intensity which we associate with the improved debundling of the nanotubes combined with the protective coating provided by the Spiro-OMeTAD coating. These novel nanohybrids have potential future applications in high-efficiency, cost-effective carbon nanotube-based organic and hybrid optoelectronics.

METHODS

Materials. CoMoCAT SG 76 SWNTs with small diameter (0.7−1.1 nm) and purity >90% were purchased from Sigma-Aldrich. Regioregular poly(3-hexylthiophene-2,5-diyl) (P3HT) with molecular weight 50 000−70 000 g mol^{-1} and poly[9,9-dioctylfluorenyl-2,7-diyl)-*co*-1,4-benzo-2,10−3-thiadiazole)] (F8BT) with molecular weight 15 000−200 000 g mol^{-1} were used as received from Rieke Metals, Inc. and American Dye Source, Inc., respectively. Spiro-OMeTAD (2,2′,7,7′-tetrakis(*N*,*N*-dimethoxyphenylamine)-9,9′-spirobifluorene) was purchased from Borun Chemicals. All solvents were purchased from Sigma-Aldrich.

Preparation of Nanohybrids. The polymer-NT (P3HT-NT/F8BT-NT) nanohybrids were prepared as described elsewhere.[15,25,26] Briefly, 6 mg of P3HT (5 mg of F8BT) was dissolved in 10 mL of chlorobenzene and homogenized in a sonic bath. Then, 3 mg of CoMoCAT SG 76 nanotubes were added to the polymer solution and the mixture was treated in an ultrasonic disintegrator for 15 min to break the SWNT bundles and hence causing effective interaction between the polymer and individual nanotubes. During sonication, the temperature of the mixture was kept constant at 25 °C. Subsequently, the mixture was centrifuged at 10 000*g* for 8 min to remove the unwrapped and bundled nanotubes. To extract the individually wrapped nanotubes and remove the excess polymer, toluene was added to the supernatant in a 1:1 ratio and left for a few hours until the aggregates were visible. The nanohybrids were then precipitated out by centrifuging at 16 000*g* for 4 min. The supernatant which contains the excess polymer was discarded and the residue was then redissolved in chlorobenzene. This purification step was repeated three times to remove the unreacted polymer. Finally, highly purified nanohybrids were redissolved in chloroform to any desired concentrations. To prepare Spiro-OMeTAD-[polymer-NT] nanohybrids, desired concentration of Spiro-OMeTAD was added to the polymer−NT solution and tip sonicated for 10 min. The resulting solution was then drop-casted on a plasma-etched quartz substrate and placed on a hot plate for about 10 s. Note that all sample preparation steps were performed in air.

Optical Absorption measurement. Absorbance measurements for the films were carried out in the wavelength range 250−1500 nm, using a PerkinElmer Lambda 9 Photospectrometer, at room temperature.

Photoluminescence Mapping. Photoluminescence excitation maps were taken using a custom build setup[26] consisting of 75 W xenon lamp focused into a monochromator, which then illuminated the nanohybrid films on a quartz substrate. The photoluminescence was collected at 90° to the excitation beam and focused into a spectrograph with a liquid nitrogen-cooled InGaAs photodiode array. The spectral response was normalized using a silicon photodiode and the instrumental response was corrected using a tungsten filament lamp of known emissivity.

AFM and SEM. For Atomic Force Microscopy and Scanning Electron Microscopy measurements, dilute solutions of polymer−NT and Spiro-OMeTAD-[polymer−NT] nanohybrids were drop-casted on a well cleaned flat silicon substrate. AFM images were taken with Autoprobe M5, in noncontact mode, with a scan rate of 0.2 Hz and 512 sample/lines. SEM was performed with a Hitachi S-4300 scanning electron microscope system.

Conflict of Interest: The authors declare no competing financial interest.

Supporting Information Available: Additional PLE maps and plots showing nanotube peak position with increasing concentration of Spiro-OMeTAD. This material is available free of charge *via* the Internet at http://pubs.acs.org.

Acknowledgment. The authors thank the Engineering and Physical Sciences Research Council for their financial support and Beate Dirks for useful discussion. J.J.S. acknowledges the University of Oxford Clarendon Fund Scholarship for financial support.

REFERENCES AND NOTES

1. Reich, S.; Thomsen, C.; Maultzsch, J. *Carbon Nanotubes: Basic Concepts and Physical Properties*; Wiley-VCH: Weinheim, 2004.
2. D'Souza, F.; Sandanayaka, A. S. D.; Ito, O. SWNT-Based Supramolecular Nanoarchitectures with Photosensitizing Donor and Acceptor Molecules. *J. Phys. Chem. Lett.* **2010**, *1*, 2586–2593.
3. Coleman, J. N.; Cadek, M.; Ryan, K. P.; Fonseca, A.; Nagy, J. B.; Blau, W. J.; Ferreira, M. S. Reinforcement of Polymers with Carbon Nanotubes. The Role of an Ordered Polymer Interfacial Region. Experiment and Modeling. *Polymer* **2006**, *47*, 8556–8561.
4. Stranks, S. D.; Weisspfennig, C.; Parkinson, P.; Johnston, M. B.; Herz, L. M.; Nicholas, R. J. Ultrafast Charge Separation at a Polymer-Single-Walled Carbon Nanotube Molecular Junction. *Nano Lett.* **2011**, *11*, 66–72.
5. Kanai, Y.; Grossman, J. C. Role of Semiconducting and Metallic Tubes in P3HT/Carbon-Nanotube Photovoltaic Heterojunctions: Density Functional Theory Calculations. *Nano Lett.* **2008**, *8*, 908–912.
6. Ren, S.; Bernardi, M.; Lunt, R. R.; Bulovic, V.; Grossman, J. C.; Gradečak, S. Toward Efficient Carbon Nanotube/P3HT Solar Cells: Active Layer Morphology, Electrical, and Optical Properties. *Nano Lett.* **2011**, *11*, 5316–5321.
7. Bindl, D. J.; Wu, M.-Y.; Prehn, F. C.; Arnold, M. S. Efficiently Harvesting Excitons from Electronic Type-Controlled Semiconducting Carbon Nanotube Films. *Nano Lett.* **2011**, *11*, 455–460.
8. Dabera, G. D. M. R.; Jayawardena, K. D. G. I.; Prabhath, M. R. R.; Yahya, I.; Tan, Y. Y.; Nismy, N. A.; Shiozawa, H.;

Sauer, M.; Ruiz-Soria, G.; Ayala, P.; *et al.* Hybrid Carbon Nanotube Networks as Efficient Hole Extraction Layers for Organic Photovoltaics. *ACS Nano* **2012**, *7*, 556–565.
9. Dissanayake, N. M.; Zhong, Z. Unexpected Hole Transfer Leads to High Efficiency Single-Walled Carbon Nanotube Hybrid Photovoltaic. *Nano Lett.* **2011**, *11*, 286–290.
10. Li, Z.; Kulkarni, S. A.; Boix, P. P.; Shi, E.; Cao, A.; Fu, K.; Batabyal, S. K.; Zhang, J.; Xiong, Q.; Wong, L. H.; *et al.* Laminated Carbon Nanotube Networks for Metal Electrode-Free Efficient Perovskite Solar Cells. *ACS Nano* **2014**, *8*, 6797–6804.
11. Habisreutinger, S. N.; Leijtens, T.; Eperon, G. E.; Stranks, S. D.; Nicholas, R. J.; Snaith, H. J. Carbon Nanotube/Polymer Composite as a Highly Stable Charge Collection Layer in Perovskite Solar Cells. *Nano Lett.* **2014**, *14*, 5561–5568.
12. Habisreutinger, S. N.; Leijtens, T.; Eperon, G. E.; Stranks, S. D.; Nicholas, R. J.; Snaith, H. J. Enhanced Hole Extraction in Perovskite Solar Cells through Carbon Nanotubes. *J. Phys. Chem. Lett.* **2014**, *5*, 4207–4212.
13. O'Connell, M. J.; Boul, P.; Ericson, L. M.; Huffman, C.; Wang, Y.; Haroz, E.; Kuper, C.; Tour, J.; Ausman, K. D.; Smalley, R. E. Reversible Water-Solubilization of Single-Walled Carbon Nanotubes by Polymer Wrapping. *Chem. Phys. Lett.* **2001**, *342*, 265–271.
14. Schuettfort, T.; Nish, A.; Nicholas, R. J. Observation of a Type II Heterojunction in a Highly Ordered Polymer–Carbon Nanotube Nanohybrid Structure. *Nano Lett.* **2009**, *9*, 3871–3876.
15. Stranks, S. D.; Yong, C.-K.; Alexander-Webber, J. A.; Weisspfennig, C.; Johnston, M. B.; Herz, L. M.; Nicholas, R. J. Nanoengineering Coaxial Carbon Nanotube-Dual-Polymer Heterostructures. *ACS Nano* **2012**, *6*, 6058–6066.
16. Stranks, S. D.; Habisreutinger, S. N.; Dirks, B.; Nicholas, R. J. Novel Carbon Nanotube-Conjugated Polymer Nanohybrids Produced By Multiple Polymer Processing. *Adv. Mater.* **2013**, *25*, 4365–4371.
17. Sprafke, J. K.; Stranks, S. D.; Warner, J. H.; Nicholas, R. J.; Anderson, H. L. Noncovalent Binding of Carbon Nanotubes by Porphyrin Oligomers. *Angew. Chem., Int. Ed.* **2011**, *50*, 2313–2316.
18. Stranks, S. D.; Sprafke, J. K.; Anderson, H. L.; Nicholas, R. J. Electronic and Mechanical Modification of Single-Walled Carbon Nanotubes by Binding to Porphyrin Oligomers. *ACS Nano* **2011**, *5*, 2307–2315.
19. Bach, U.; Lupo, D.; Comte, P.; Moser, J. E.; Weissortel, F.; Salbeck, J.; Spreitzer, H.; Gratzel, M. Solid-State Dye-Sensitized Mesoporous TiO_2 Solar Cells with High Photon-to-Electron Conversion Efficiencies. *Nature* **1998**, *395*, 583–585.
20. Green, M. A.; Ho-Baillie, A.; Snaith, H. J. The Emergence of Perovskite Solar Cells. *Nat. Photonics* **2014**, *8*, 506–514.
21. Jeon, N. J.; Noh, J. H.; Kim, Y. C.; Yang, W. S.; Ryu, S.; Seok, S. I. Solvent Engineering for High-Performance Inorganic-Organic Hybrid Perovskite Solar Cells. *Nat. Mater.* **2014**, *13*, 897–903.
22. Lee, M. M.; Teuscher, J.; Miyasaka, T.; Murakami, T. N.; Snaith, H. J. Efficient Hybrid Solar Cells Based on Meso-Superstructured Organometal Halide Perovskites. *Science* **2012**, *338*, 643–647.
23. Zhou, H.; Chen, Q.; Li, G.; Luo, S.; Song, T.-b.; Duan, H.-S.; Hong, Z.; You, J.; Liu, Y.; Yang, Y. Interface Engineering of Highly Efficient Perovskite Solar Cells. *Science* **2014**, *345*, 542–546.
24. Burschka, J.; Pellet, N.; Moon, S. J.; Humphry-Baker, R.; Gao, P.; Nazeeruddin, M. K.; Gratzel, M. Sequential Deposition as a Route to High-Performance Perovskite-Sensitized Solar Cells. *Nature* **2013**, *499*, 316–319.
25. Schuettfort, T.; Snaith, H. J.; Nish, A.; Nicholas, R. J. Synthesis and Spectroscopic Characterization of Solution Processable Highly Ordered Polythiophene–Carbon Nanotube Nanohybrid Structures. *Nanotechnology* **2010**, *21*, 025201.
26. Nish, A.; Hwang, J.-Y.; Doig, J.; Nicholas, R. J. Highly Selective Dispersion of Single-Walled Carbon Nanotubes using Aromatic Polymers. *Nat. Nanotechnol.* **2007**, *2*, 640–646.
27. Bachilo, S. M.; Strano, M. S.; Kittrell, C.; Hauge, R. H.; Smalley, R. E.; Weisman, R. B. Structure-Assigned Optical Spectra of Single-Walled Carbon Nanotubes. *Science* **2002**, *298*, 2361–2366.
28. Li, L.-J.; Nicholas, R. J.; Deacon, R. S.; Shields, P. A. Chirality Assignment of Single-Walled Carbon Nanotubes with Strain. *Phys. Rev. Lett.* **2004**, *93*, 156104.
29. Leeuw, T. K.; Tsyboulski, D. A.; Nikolaev, P. N.; Bachilo, S. M.; Arepalli, S.; Weisman, R. B. Strain Measurements on Individual Single-Walled Carbon Nanotubes in a Polymer Host: Structure-Dependent Spectral Shifts and Load Transfer. *Nano Lett.* **2008**, *8*, 826–831.
30. Yang, L.; Anantram, M. P.; Han, J.; Lu, J. P. Band-Gap Change of Carbon Nanotubes: Effect of Small Uniaxial and Torsional strain. *Phys. Rev. B* **1999**, *60*, 13874–13878.
31. Heeg, S.; Malić, E.; Casiraghi, C.; Reich, S. Quantitative Composition of a Single-Walled Carbon Nanotube Sample: Raman Scattering *versus* Photoluminescence. *Phys. Status Solidi B* **2009**, *246*, 2740–2743.
32. Hwang, J.-Y.; Nish, A.; Doig, J.; Douven, S.; Chen, C.-W.; Chen, L.-C.; Nicholas, R. J. Polymer Structure and Solvent Effects on the Selective Dispersion of Single-Walled Carbon Nanotubes. *J. Am. Chem. Soc.* **2008**, *130*, 3543–3553.
33. Valavala, P. K.; Banyai, D.; Seel, M.; Pati, R. Self-Consistent Calculations of Strain-Induced Band Gap Changes in Semiconducting Carbon nanotubes. *Phys. Rev. B* **2008**, *78*, 235430.
34. Yang, L.; Han, J. Electronic Structure of Deformed Carbon Nanotubes. *Phys. Rev. Lett.* **2000**, *85*, 154–157.
35. Gartstein, Y. N.; Zakhidov, A. A.; Baughman, R. H. Mechanical and Electromechanical Coupling in Carbon Nanotube Distortions. *Phys. Rev. B* **2003**, *68*, 115415.